

## Experimental violation of a Bell inequality with two different degrees of freedom of entangled particle pairs

Xiao-song Ma,<sup>1,2</sup> Angie Qarry,<sup>1</sup> Johannes Kofler,<sup>1,2</sup> Thomas Jennewein,<sup>1</sup> and Anton Zeilinger<sup>1,2</sup>  
<sup>1</sup>*Institute for Quantum Optics and Quantum Information (IQOQI), Austrian Academy of Sciences, Boltzmanngasse 3,  
 A-1090 Vienna, Austria*

<sup>2</sup>*Faculty of Physics, University of Vienna, Boltzmanngasse 5, A-1090 Vienna, Austria*

(Received 16 October 2008; published 20 April 2009)

We demonstrate hybrid entanglement of photon pairs via the experimental violation of a Bell inequality with two different degrees of freedom (DOF), namely, the path (linear momentum) of one photon and the polarization of the other photon. Hybrid entangled photon pairs are created by spontaneous parametric down conversion and coherent polarization to path conversion for one photon. For that photon, path superposition is analyzed, and polarization superposition for its twin photon. The correlations between these two measurements give an  $S$  parameter of  $S=2.653 \pm 0.027$  in a Clauser-Horne-Shimony-Holt inequality and thus violate local realism for two different DOF by more than 24 standard deviations. This experimentally supports the idea that entanglement is a fundamental concept which is indifferent to the specific physical realization of Hilbert space.

DOI: [10.1103/PhysRevA.79.042101](https://doi.org/10.1103/PhysRevA.79.042101)

PACS number(s): 03.65.Ud, 42.50.Xa

The assumption of local realism led Einstein, Podolsky, and Rosen (EPR) to argue that quantum mechanics is not a complete theory [1]. In 1951 Bohm [2] discussed a system of two spatially separated and entangled spin- $\frac{1}{2}$  particles in order to illustrate the essential features of the EPR paradox. All hidden-variable theories based on the joint assumptions of locality and realism are at variance with the predictions of quantum physics, as shown by the violation of the famous Bell inequalities [3] using entangled spin- $\frac{1}{2}$  particles. Since the formulation of the Bell inequalities and later of the Clauser-Horne-Shimony-Holt (CHSH) inequality [4], numerous experiments based on polarization-entangled photons have been performed that verified the quantum-mechanical predictions [5–7]. Besides the polarization of photons, there are theoretical proposals to test Bell's inequality with the other degrees of freedom (DOF), e.g., using the momentum [8–10] or the emission time [11] of entangled photon pairs. The experimental violation of Bell's inequality based on the momentum and phase was demonstrated by Rarity and Tapster [12], while the time-bin entanglement has been employed in the fiber-based quantum cryptography and communication [13].

Here we follow the proposal in [14] and experimentally realize *hybrid* entanglement, which is the entanglement between *different* degrees of freedom of a particle *pair*. We specifically demonstrate the hybrid entanglement between the polarization of a photon from a photon pair and the path (momentum) of its twin. We want to stress that hybrid entanglement is in principle different from so-called hyperentanglement [15]. A hyperentangled state is a tensor product of entangled states in each *individual* DOF. Therefore, there is no entanglement between different DOF. A *hybrid-entangled state cannot be factorized into states of individual DOF only*. In a hyperentangled state of, say, two particles joint properties of the same degree of freedom are well defined at the expense of defining individual properties. The joint properties allow to make predictions for experimental situations where both particles are measured in one and the same degree of freedom. With hybrid entanglement the situ-

ation is different. There, the defined joint properties are such that they link one degree of freedom of one particle with another degree of freedom of the other particle, where those degrees may even be defined in Hilbert spaces of different dimensionalities as, e.g., polarization and linear momentum. While the Hilbert-space structure of quantum mechanics demands the existence of such hybrid-entangled states, they have not been shown experimentally until now.

The entanglement between the polarization and the momentum DOF [16,17] as well as between the polarization and the orbital angular-momentum DOF [18] of a *single* photon, and between the spatial and spin DOF of a *single* neutron [19] was demonstrated experimentally. The idea to convert the polarization entanglement to path entanglement of a photon pair was realized in [20]. There have also been experimental realizations of two-photon four-qubit cluster states with entanglement between both path and polarization [21,22]. On the other hand, entanglement between the same degree of freedom of different physical systems has also been realized. In many atom-photon experiments entanglement has been demonstrated between the spin of the atom state and the spin (i.e., polarization) of the photon [23].

In this article, we demonstrate hybrid entanglement of photon pairs between two different degrees of freedom, namely, path (linear momentum) and polarization, via the experimental violation of the CHSH inequality. Normally, in the case of the polarization entanglement of a photon pair, the maximum violation of the CHSH inequality is established with the polarizers oriented at  $(-22.5^\circ, 22.5^\circ)$  at Bob's side and  $(0^\circ, 45^\circ)$  at Alice's side, while in the case of path entanglement it is established with the phase shift at  $(-45^\circ, 45^\circ)$  at Bob's side and  $(0^\circ, 90^\circ)$  at Alice's side. In order to maximally violate the CHSH inequality for the hybrid entanglement, the polarizer at Bob's side (photon B) is oriented at the *angles* of  $(-22.5^\circ, 22.5^\circ)$  and the phase shifter at Alice's side (photon A) is adjusted at the *phase* of  $(0^\circ, 90^\circ)$ . This manifests the hybrid nature of our entangled photon pairs. A very important feature of the present experiment is, that the interferometer—the analyzer of the path

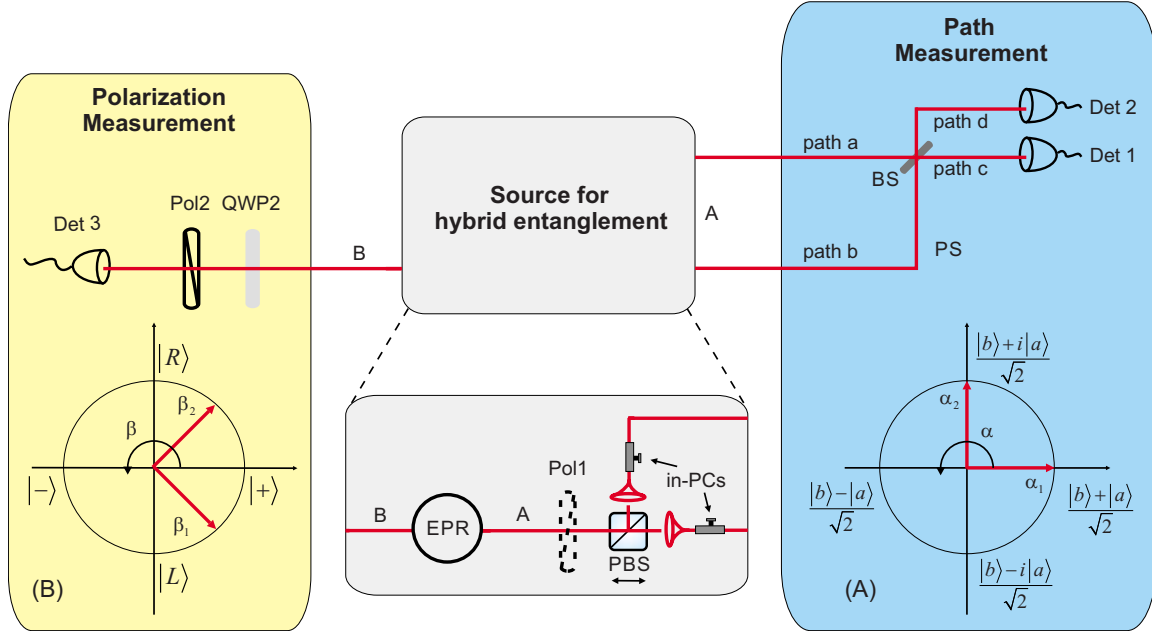


FIG. 1. (Color online) Experimental Setup. Polarization-entangled photon pairs are generated in an EPR-Bell state via spontaneous parametric down conversion (SPDC). A picosecond-pulsed Nd:vanadate laser emitting light at the wavelength of 355 nm after frequency tripling (repetition rate of 76 MHz and average power of 200 mW) pumps a  $\beta$ -barium borate ( $\beta$ -BBO) crystal in a cross rings type-II scheme of SPDC [24]. Good spectrum and spatial mode overlapping is achieved by using interference filters with 1 nm bandwidth centered around 710 nm and by collecting the entangled photon pairs into single-mode fibers [25]. In order to create the hybrid-entangled state (1), the source also consists of a polarizing beam splitter, two in-line polarization controllers (in-PCs) and an additional linear polarizer (Pol1) [see main text for details]. The photon in spatial mode A is directed toward the interferometric path measurement setup. We combine both paths on a single-mode fiber beam splitter and the length of the whole interferometer is about 2 m. The phase scanner is realized via position change ( $x$ ) of the PBS. The photon in spatial mode B is directed toward the polarization measurement setup. It consists of a quarter-wave plate (QWP2) and a linear polarizer (Pol2) with the transmission axis oriented along angle  $\phi$ , which together allow to project photon B into the desired polarization states. Both photon A and photon B are detected by multimode fiber coupled silicon avalanche photodiodes (Det 1, 2, 3). Photon A is analyzed in the superposition of the two path states along  $\alpha_1$ ,  $\alpha_2$ , and their orthogonal directions on its Bloch sphere shown in the inset (a). Photon B is analyzed in the superposition of the polarization states along directions  $\beta_1$ ,  $\beta_2$ , and their orthogonal directions on its Bloch sphere shown in the inset (b).

DOF—is calibrated strictly locally and before the correlation measurements. Therefore, it is possible to independently choose the settings on each side. We also applied this specific hybrid entanglement to perform a quantum eraser experiment under strict (Einstein) locality condition, which will be presented elsewhere.

The scheme of our experiment is shown in Fig. 1. First, we create the polarization-entangled EPR-Bell state  $|\Phi^+\rangle = \frac{1}{\sqrt{2}}(|H\rangle_A|V\rangle_B + |V\rangle_A|H\rangle_B)$ , where  $|H\rangle$  and  $|V\rangle$  denote the horizontal and vertical linearly polarized quantum states respectively, and A and B index the spatial modes of the photons. Next we will investigate how the quantum state  $|\Phi^+\rangle$  evolved in the setup. A polarizing beam splitter (PBS) transmits the horizontal and reflects the vertical polarization state of photon A. Thus, the PBS acts as a deterministic polarization-momentum converter. Two in-line polarization controllers (in-PCs) are used to rotate the orthogonal polarization states of photon A in paths a and b ( $|H\rangle_{Aa}$  and  $|V\rangle_{Ab}$ ) to an identical one [ $|\theta, \gamma\rangle_{Aa}$  and  $|\theta, \gamma\rangle_{Ab}$ , where  $|\theta, \gamma\rangle_{Aa} = |\theta, \gamma\rangle_{Ab} = \cos \theta |H\rangle + \exp(i\gamma) \sin \theta |V\rangle$ ] and thus eliminate the polarization distinguishability of the two paths. Hence from now on we will ignore the polarization of photon A and label it with its path quantum states, where

$|a\rangle_A \equiv |\theta, \gamma\rangle_{Aa}$  and  $|b\rangle_A \equiv |\theta, \gamma\rangle_{Ab}$ . Therefore, the source creates the hybrid-entangled state between the path of photon A and the polarization of photon B,

$$|\Phi_{\text{hybrid}}^+\rangle = \frac{1}{\sqrt{2}}(|b\rangle_A|V\rangle_B + |a\rangle_A|H\rangle_B). \quad (1)$$

The superposition states of the two paths of photon A are varied and analyzed by a modified Mach-Zehnder interferometer. After a phase scanner (PS) and beam splitter (BS), the state becomes  $|\Phi_{\text{hybrid}}^{+'}\rangle = \frac{1}{\sqrt{2}}[(|d\rangle_A + i|c\rangle_A)|V\rangle_B + \exp(i\alpha)(|c\rangle_A + i|d\rangle_A)|H\rangle_B]$ . On photon B's side, by proper polarization projection, the hybrid-entangled state becomes

$$\begin{aligned} |\Phi_{\text{hybrid}}^{+''}\rangle = & \frac{1}{2}(e^{i\kappa_1}\sqrt{1 + \sin(\alpha + \beta)}|c\rangle_A|\beta\rangle_B \\ & + e^{i\kappa_2}\sqrt{1 - \sin(\alpha + \beta)}|d\rangle_A|\beta\rangle_B \\ & + e^{i\kappa_3}\sqrt{1 - \sin(\alpha + \beta)}|c\rangle_A|\beta^\perp\rangle_B \\ & + e^{i\kappa_4}\sqrt{1 + \sin(\alpha + \beta)}|d\rangle_A|\beta^\perp\rangle_B). \end{aligned} \quad (2)$$

Here,  $|\beta\rangle_B = \frac{1}{\sqrt{2}}[|H\rangle_B + \exp(i\beta)|V\rangle_B]$  and  $|\beta^\perp\rangle_B$

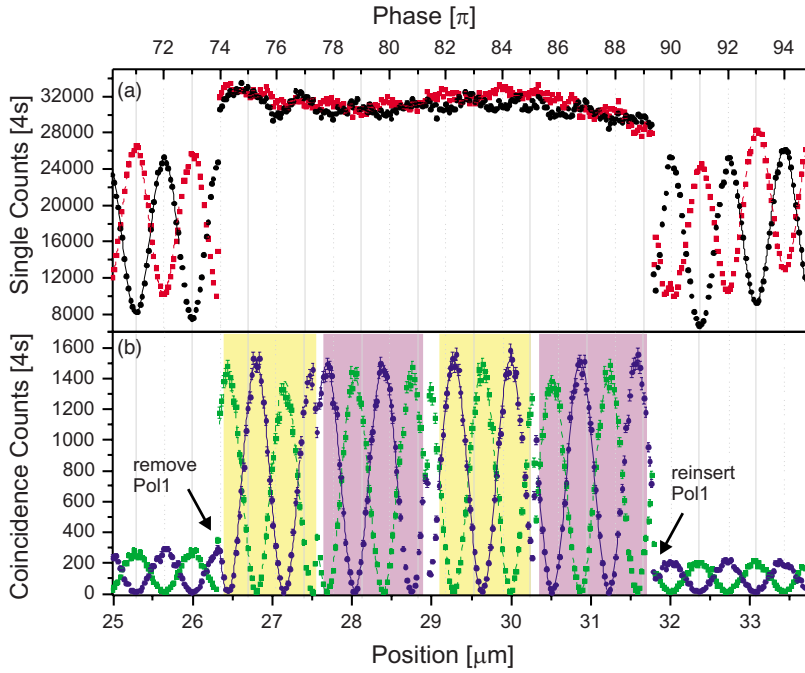


FIG. 2. (Color online) Experimental results. (a) The single counts of Det1 (red square dots) and Det2 (black circular dots) are fitted with sinusoidal curves (red dash and black solid lines for Det1 and Det2, respectively) at the beginning and the end in order to calibrate the local phase of the Mach-Zehnder interferometer. (b) The coincidence counts between Det1 and Det3 (green square dots) and Det2 with Det3 (blue circular dots) and the corresponding sinusoidal fits (green dash and blue solid lines, respectively). They are used to construct the correlation coefficients in order to violate the Bell inequality. Alternating color (gray) shadings are designating the different settings of Pol2. The actions of removing and reinserting Pol1 are identified with arrows. The error bars are the square roots of the corresponding counts.

$= \frac{1}{\sqrt{2}}[|H\rangle_B - \exp(i\beta)|V\rangle_B]$ , respectively,  $|c\rangle_A$  and  $|d\rangle_A$  are the spatial modes after the BS, and  $\kappa_1, \kappa_2, \kappa_3$ , and  $\kappa_4$  are the phases of the four different coincidence terms which are not important in the present experiment.

On the photon A side, we tune the local phase difference between the two path quantum states ( $|a\rangle_A$  and  $|b\rangle_A$ ), which corresponds to the phase  $\alpha$  of the interferometer in Eq. (2). Scanning this phase  $\alpha$  with PS to ( $\alpha_1 \equiv 0^\circ, \alpha_2 \equiv 90^\circ, \alpha_1^\perp \equiv 180^\circ, \alpha_2^\perp \equiv -90^\circ$ ) and detecting the photon with Det1 and Det2 is like projecting the path states of photon A into the states  $|\alpha_1\rangle \equiv \frac{1}{\sqrt{2}}(|b\rangle + |a\rangle)$ ,  $|\alpha_2\rangle \equiv \frac{1}{\sqrt{2}}(|b\rangle + i|a\rangle)$ ,  $|\alpha_1^\perp\rangle \equiv \frac{1}{\sqrt{2}}(|b\rangle - |a\rangle)$ , and  $|\alpha_2^\perp\rangle \equiv \frac{1}{\sqrt{2}}(|b\rangle - i|a\rangle)$ , respectively, as shown in the inset of Fig. 1(A). The relation between the position  $x$  of the PBS and the phase of the interferometer  $\alpha$  is  $x = \frac{\alpha\lambda}{2\pi}$ . On the photon B side, we can tune the phase between the two polarization quantum states ( $|H\rangle_B$  and  $|V\rangle_B$ ), which corresponds to the phase  $\beta$  in Eq. (2). By setting the QWP2 at  $-45^\circ$  oriented relative to the horizontal direction and rotating Pol2 such that  $\beta$  is equal to ( $\beta_1 \equiv -45^\circ, \beta_2 \equiv 45^\circ, \beta_1^\perp \equiv 135^\circ, \beta_2^\perp \equiv -135^\circ$ ), we are able to project the polarization states of photon B into the desired states  $|\beta_1\rangle = \frac{1}{\sqrt{2}}[|H\rangle_B + \frac{1}{\sqrt{2}}(1-i)|V\rangle_B]$ ,  $|\beta_2\rangle = \frac{1}{\sqrt{2}}[|H\rangle_B + \frac{1}{\sqrt{2}}(1+i)|V\rangle_B]$ ,  $|\beta_1^\perp\rangle = \frac{1}{\sqrt{2}}[|H\rangle_B + \frac{1}{\sqrt{2}}(-1+i)|V\rangle_B]$ , and  $|\beta_2^\perp\rangle = \frac{1}{\sqrt{2}}[|H\rangle_B + \frac{1}{\sqrt{2}}(-1-i)|V\rangle_B]$ , respectively, as shown in the inset (B) of Fig. 1. The relation between the orientation angle of Pol2 and  $\beta$  is  $\phi = -\frac{\beta}{2}$ .

Experimentally, we measured in three steps: (I) we inserted Pol1 oriented at  $45^\circ$  into the setup. Then the entanglement is erased and photon A is in a coherent superposition of taking path a ( $|a\rangle_A$ ) or path b ( $|b\rangle_A$ ). In Fig. 2(a), we show the single counts of Det1 (red square dots) and Det2 (black circular dots). Two oppositely modulated data curves, as a function of the relative phase change of the two paths, enable us to find the absolute value of the local phase of the interferometer. We define  $\alpha \equiv 2n\pi$  ( $n$  is an integer) when Det2 has maximum counts. Thus, the coincidence counts of Det1

with Det3 (green square dots in Fig. 2) and Det2 with Det3 (blue circular dots in Fig. 2) are oscillating in phase with the corresponding single counts.

(II) We remove Pol1 and measure the coincidence counts of Det1 with Det3 and Det2 with Det3. From these coincidence counts we construct the correlation coefficients for the violation of the Bell inequality. When we take out Pol1, there are two important features in Fig. 2. First, the oscillations of single counts ceased and this can be explained by Eq. (2). For instance, one can calculate the probability amplitude for  $|c\rangle_A$ , which is a sum of two oppositely modulated sinusoidal functions. Thus, the single counts of Det1 are insensitive to the phase change both “locally” ( $\alpha$ ) and “nonlocally” ( $\beta$ ). The same reasoning applies to the single counts of Det2 as well. Second, the coincidence counts behave differently relative to the single counts. The coincidence counts keep oscillating as we are scanning the local phase ( $\alpha$ ) and the oscillating amplitude increases. The reason for the increase is that we first aligned Pol2 at  $-22.5^\circ$  and Pol1 at  $-45^\circ$  and theoretically the corresponding coincidence counts are only 0.146 of the coincidence counts of the case when Pol1 is removed. Experimentally we found that was about 0.19. Moreover, there is a phase jump between the oscillating curves of the coincidence counts of the two cases with or without Pol1. For example, the coincidence counts between Det1 and Det3 are proportional to the joint probability for detecting photon A in path c ( $|c\rangle_A$ ) and detecting the polarization of photon B along  $\beta$ , which is proportional to  $1 + \sin(\alpha)$  with Pol1 and proportional to  $1 + \sin(\alpha + \beta)$  without Pol1. Experimentally, as stated above, we first align Pol2 at  $-22.5^\circ$  and Pol1 at  $-45^\circ$ , which corresponds to a phase difference of  $225^\circ$ . The measured value is  $230^\circ$ . This allows to quantitatively explain that the coincidence counts are expected to be 0.18 of the coincidence of the case when Pol1 is removed. Then we scan the local phase continuously and set the orientation angle of Pol2 to ( $-22.5^\circ, 22.5^\circ, 67.5^\circ, 112.5^\circ$ ) sequentially, which corre-

sponds to  $(\beta_2, \beta_1, \beta_2^\perp, \beta_1^\perp)$ . These four different settings are designated with four alternated color (gray) shaded regions in Fig. 2(b). Due to the reasons stated above, there are phase jumps of the coincidence counts between the different settings of Pol2. The phase jumps between the neighboring regions are expected to be  $90^\circ$ , while  $89.2^\circ$ ,  $92.4^\circ$ , and  $86.8^\circ$  were the measured values, respectively. These four regions of the data are enough to construct the correlation coefficients and to violate the Bell inequality.

(III) After we get the coincidence data, we insert Pol1 back again to determine the phase drift during the whole measurement cycle. We get a  $2.0^\circ$  phase difference on average. Without subtracting the accidental coincidence counts, the interference visibilities of the coincidence counts are above 96% for all four settings. The wavelength of all the fits (including single counts and coincidence counts) is fixed to 708.6 nm.

Given a setting pair  $(\alpha_i, \beta_j)$ , which are the orientations of the vectors of the analyzers on the Bloch sphere of photon A and B, respectively, the correlation coefficients are defined as

$$E(\alpha_i, \beta_j) = \frac{C(\alpha_i, \beta_j) + C(\alpha_i^\perp, \beta_j^\perp) - C(\alpha_i^\perp, \beta_j) - C(\alpha_i, \beta_j^\perp)}{C(\alpha_i, \beta_j) + C(\alpha_i^\perp, \beta_j^\perp) + C(\alpha_i^\perp, \beta_j) + C(\alpha_i, \beta_j^\perp)}, \quad (3)$$

where  $C(\alpha_i, \beta_j)$  and  $C(\alpha_i^\perp, \beta_j)$  [ $C(\alpha_i^\perp, \beta_j^\perp)$  and  $C(\alpha_i, \beta_j^\perp)$ ] are the coincidence counts of Det1 with Det3 and Det2 with Det3, respectively, given the local phase of interferometer on photon A side is  $\alpha_i(\alpha_i^\perp)$  and the orientation of polarizer on photon B side is such that  $\beta = \beta_j(\beta_j^\perp)$  with  $i, j = 1, 2$ . From the state (2), it follows that  $E(\alpha_i, \beta_j) = \sin(\alpha_i + \beta_j)$ . If local realism is valid, such correlation coefficients must satisfy the CHSH inequality,

$$S = -E(\alpha_1, \beta_1) + E(\alpha_1, \beta_2) + E(\alpha_2, \beta_1) + E(\alpha_2, \beta_2) \leq 2. \quad (4)$$

But quantum mechanics predicts values up to  $2\sqrt{2}$ .

The correlation coefficients are calculated from the data from Fig. 2(b), which are

$$E(\alpha_1, \beta_1) = E(28.140 \mu\text{m}, 22.5^\circ) = -0.666 \pm 0.014,$$

$$E(\alpha_1, \beta_2) = E(28.291 \mu\text{m}, 22.5^\circ) = 0.671 \pm 0.014,$$

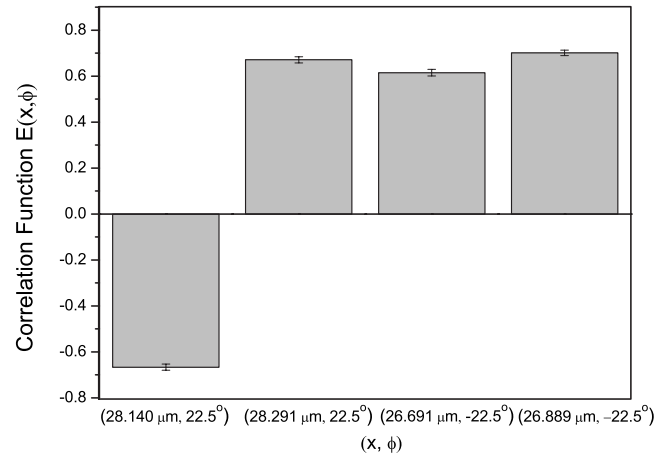


FIG. 3. Four correlation functions of the CHSH inequality for four different settings. Operationally, the setting on photon A side is given by the position of the phase scanner  $x$  and on photon B side it is the orientation of the polarizer  $\phi$ . This manifests the hybrid nature of the entangled photon pair. The error bars represent its statistical errors.

$$E(\alpha_2, \beta_1) = E(26.691 \mu\text{m}, -22.5^\circ) = 0.615 \pm 0.014,$$

$$E(\alpha_2, \beta_2) = E(26.889 \mu\text{m}, -22.5^\circ) = 0.701 \pm 0.012,$$

respectively, as shown in Fig. 3. The  $S$  parameter calculated from those four correlation coefficients equals to  $S = 2.653 \pm 0.027$ , which violates the classical bound ( $|S| = 2$ ) by more than 24 standard deviations.

Hybrid entanglement is not only of fundamental interest. It also could be useful in quantum information processing, e.g., the quantum repeater [26]. It is not limited to the case of path (linear momentum) and polarization, as we have shown in this paper, but also should be possible for other degrees of freedom, e.g., frequency, orbital angular momentum etc. of photons.

We are grateful to R. Ursin, Č. Brukner, and M. Żukowski for discussions. We acknowledge support by the IST funded Integrated Project QAP (Contract No. 015846) of the European Commission and the Doctoral Program CoQuS of the Austrian Science Foundation (FWF).

[1] A. Einstein, B. Podolsky, and N. Rosen, *Phys. Rev.* **47**, 777 (1935).  
 [2] D. Bohm, *Quantum Theory* (Prentice-Hall, Englewood Cliffs, NJ, 1951).  
 [3] J. S. Bell, *Physics* **1**, 195 (1964).  
 [4] J. F. Clauser, M. A. Horne, A. Shimony, and R. A. Holt, *Phys. Rev. Lett.* **23**, 880 (1969).  
 [5] S. J. Freedman and J. F. Clauser, *Phys. Rev. Lett.* **28**, 938 (1972).  
 [6] A. Aspect, P. Grangier, and G. Roger, *Phys. Rev. Lett.* **49**, 91 (1982).

[7] G. Weihs, T. Jennewein, C. Simon, H. Weinfurter, and A. Zeilinger, *Phys. Rev. Lett.* **81**, 5039 (1998).  
 [8] M. A. Horne and A. Zeilinger, *Proceedings of the Symposium on the Foundations of Modern Physics* (World Scientific, Singapore, 1985).  
 [9] M. A. Horne, A. Shimony, and A. Zeilinger, *Phys. Rev. Lett.* **62**, 2209 (1989).  
 [10] M. Żukowski and J. Pykacz, *Phys. Lett. A* **127**, 1 (1988).  
 [11] J. D. Franson, *Phys. Rev. Lett.* **62**, 2205 (1989).  
 [12] J. G. Rarity and P. R. Tapster, *Phys. Rev. Lett.* **64**, 2495 (1990).

- [13] N. Gisin, G. Ribordy, W. Tittel, and H. Zbinden, *Rev. Mod. Phys.* **74**, 145 (2002).
- [14] M. Żukowski and A. Zeilinger, *Phys. Lett. A* **155**, 69 (1991).
- [15] J. T. Barreiro, N. K. Langford, N. A. Peters, and P. G. Kwiat, *Phys. Rev. Lett.* **95**, 260501 (2005).
- [16] D. Boschi, S. Branca, F. De Martini, L. Hardy, and S. Popescu, *Phys. Rev. Lett.* **80**, 1121 (1998).
- [17] M. Michler, H. Weinfurter, and M. Żukowski, *Phys. Rev. Lett.* **84**, 5457 (2000).
- [18] J. T. Barreiro, T.-C. Wei, and P. G. Kwiat, *Nat. Phys.* **4**, 282 (2008).
- [19] Y. Hasegawa, R. Loidl, G. Badurek, M. Baron, and H. Rauch, *Nature (London)* **425**, 45 (2003).
- [20] D. V. Strekalov, T. B. Pittman, A. V. Sergienko, Y. H. Shih, and P. G. Kwiat, *Phys. Rev. A* **54**, R1 (1996).
- [21] G. Vallone, E. Pomarico, P. Mataloni, F. De Martini, and V. Berardi, *Phys. Rev. Lett.* **98**, 180502 (2007).
- [22] K. Chen, C.-M. Li, Q. Zhang, Y.-A. Chen, A. Goebel, S. Chen, A. Mair, and J.-W. Pan, *Phys. Rev. Lett.* **99**, 120503 (2007).
- [23] J. M. Raimond, M. Brune, and S. Haroche, *Rev. Mod. Phys.* **73**, 565 (2001).
- [24] P. G. Kwiat, K. Mattle, H. Weinfurter, A. Zeilinger, A. V. Sergienko, and Y. Shih, *Phys. Rev. Lett.* **75**, 4337 (1995).
- [25] C. Kurtsiefer, M. Oberparleiter, and H. Weinfurter, *Phys. Rev. A* **64**, 023802 (2001).
- [26] L. M. Duan, M. D. Lukin, J. I. Cirac, and P. Zoller, *Nature (London)* **414**, 413 (2001).